1990

Correlation-Dimension Calculations for Broadband Intensity Fluctuations in Emission from a Heavily Saturated Source of Amplified Spontaneous Emission

B. Das

Alfonso M. Albano
Bryn Mawr College, aalbano@brynmawr.edu

N. B. Abraham

Correlation-dimension calculations for broadband intensity fluctuations in emission from a heavily saturated source of amplified spontaneous emission

B. Das,* A. M. Albano, and N. B. Abraham

Department of Physics, Bryn Mawr College, Bryn Mawr, Pennsylvania 19010-2899
(Received 22 May 1989; revised manuscript received 2 March 1990)

Broadband intensity fluctuations from a heavily saturated source of amplified spontaneous emission (ASE) operating on the 3.51-μm transition of xenon show no evidence of a dynamical origin represented by a low-dimensional underlying chaotic attractor. The broadband coupled-mode fluctuations in ASE thus seem to be stochastic when contrasted with the recently reported deterministic nature of similar broadband fluctuations of single-mode lasers operating on the same transition.

I. INTRODUCTION

Spontaneous emission from a collection of independent incoherently excited atoms is a random stochastic process. As a sum of many randomly phased contributions from different atoms, spontaneous emission has a Gaussian field amplitude probability distribution function and an exponential intensity probability distribution function (IPDF) in its fluctuations, just as for thermal radiation.[1] Amplified spontaneous emission (ASE), whose only source is the spontaneously emitted radiation within the optical amplifier, also has Gaussian amplitude statistics when the amplifier gain is linear.[1] However, since the gain becomes nonlinear when the intensity reaches a level at which stimulated emission reduces the number of excited atoms, statistical properties of the emitted radiation are significantly changed when an appreciable portion of the intensity fluctuations approach this characteristic saturation intensity.

In contrast, the spectral properties of ASE change in both the linear and nonlinear regimes. The spectral width decreases significantly with increasing amplification while the process remains linear. The spectral width decreases more slowly as saturation sets in for a homogeneously broadened medium while it increases as the gain saturates for an inhomogeneously broadened medium. Experimental measurements and theoretical analyses confirm these characteristics.[2-7]

When only a single mode of the radiation field interacts with the medium, gain saturation tends to reduce the variance of the fluctuations, as is also true in a single-mode laser when it is brought above threshold. In ASE, however, competition between different radiation modes for the finite energy supplied at a constant rate to the excited medium causes fluctuations in each mode to persist even under the condition of heavy gain saturation.

Nevertheless, even in the presence of mode competition, as the gain saturates one expects that the amplitude statistics should be different from the Gaussian statistics of thermal sources. Theoretical analyses and experimental measurements have shown unambiguously that there is a significant reduction of the fluctuations of each mode of an ASE source. However, it is also found that the saturation effects reach a limit in which the IPDF of each mode reaches a shape which depends on the number of modes present.[8-14] The limiting IPDF's found for simple rate equation models[13] obey negative polynomial distributions whose power depends only on the number of modes. The IPDF's converge to that of a thermal distribution when the number of modes approaches infinity. Because of the coupling of the modes, the intensity fluctuations of two orthogonally polarized components of the output from one end of an ASE tube were found to be significantly anticorrelated in a heavily saturated medium but were uncorrelated in an unsaturated medium.[15,16]

Under heavily saturated conditions the ASE output shows some evidence of nonstochastic behavior in the form of ringing in the intensity following large ASE pulses.[17] This is usually assumed to be correlated with coherent evolution of the collective material polarizations as described by a Bloch vector. If this is the explanation in our case, the ringing represents a kind of superfluorescent emission which clearly is not found in the emission from an unsaturated medium at the same excitation density. It is then pertinent to ask whether there is long-term dynamical behavior in the coherent ringing which can be used to distinguish it from the stochastic random intensity fluctuations of spontaneous emission of an unsaturated optical amplifier.

In addition, our preliminary reports of this work[18] led Hopf to an analysis[19] of situations under which chaotic behavior might be induced in a saturating laser amplifier. His analysis concluded that there might be spatial chaos under circumstances of a quasiperiodic input. However, for our experimental conditions, even with high saturation, he suggested that the time-dependent output would remain stochastic.

Because of the puzzling mixture of partially dynamical behavior that we have observed and which Hopf predicted, we undertook a more systematic study than that described in Ref. 18 in order to more completely characterize the experimental situation. We report the results of that search for evidence of deterministic chaos in the dynamical behavior underlying the ASE fluctuations from a heavily saturated source. During the past decade chaotic behavior has been identified in a wide variety of

seemingly unpredictable and seemingly random phenomena in hydrodynamic, chemical, biological, optical, and electronic systems.[20-26] The identification has sometimes been qualitative, as in the observation of one of a small number of universal routes to chaotic behavior. More quantitative measures have also been used to characterize the complicated signals which have broadband power spectra in order to verify that they are truly chaotic. These methods can identify when the signal arises from chaotic behavior corresponding to motion on a low-dimensional "strange attractor," so-called because the system is found to have settled into a particular ordered subset of the possible values in its phase space. Deterministic processes[27] are those for which there are definite prescriptions for all their future behavior based on present or past information. However, it is possible for a deterministic system to evolve over long times in an irregular fashion, such that the specific future is unpredictable in practice because of uncertainties in precisely specifying the system and its very sensitive dependence on the initial conditions. The evolution of these systems, in principle, is completely determined by the initial conditions and the prescribed equations of motions. It is this type of deterministic behavior that is used to define deterministic chaos. This is different from stochastic irregular behavior resulting from the combination of an extremely large number of independent variables. A stochastic random process can be described only in terms of average properties determined by its probability distribution. Hence spectral studies are not suitable for detailed classification or comparison of different kinds of complex behavior or even for the discrimination between deterministic chaos and purely stochastic noise.

Quantitative methods can be used to analyze digitized time series of one of the variables to differentiate stochastic noise from deterministic chaos.[28-31] These methods also have been refined, thereby reducing the original requirement of large data sets, and making them applicable for data sets blurred by noise. The distinction of noise from chaos has been made possible by reliable estimates of quantities such as dimensions,[28-31] metric entropies,[29,31] and Lyapunov exponents.[30] These quantities provide a quantitative means of following the system as it evolves from one kind of behavior to another. Moreover, the dimensions defined for an attractor provide estimates of the number of independent variables that may be ultimately needed to model the dynamics.

II. CORRELATED-DIMENSION CALCULATION—THEORETICAL BACKGROUND

The correlation dimension is the most widely used measure of chaotic behavior because of the relative ease with which it can be calculated from a time series. The calculation of correlation dimension (or order two information dimension) can be performed using the algorithms developed by Grassberger and Procaccia.[29,31] From each of the sets of N numbers v_i $(i = 1, 2, \ldots, N)$, one forms m-dimensional time delay

vectors $\mathbf{x}_j \equiv (v_j, v_{j+1}, \ldots, v_{j+m-1})$ and evaluates the correlation integral

$$C_m(\epsilon) \equiv \lim_{N \to \infty} \frac{1}{N(N-1)} \sum_{j \neq i = 1}^{N} \Theta(\epsilon - |\mathbf{x}_i - \mathbf{x}_j|) .$$

Here Θ is the Heaviside function. The correlation dimension is then given by

$$D_2 = \lim_{\epsilon \to 0} \lim_{m \to \infty} \frac{\ln C_m(\epsilon)}{\ln \epsilon} .$$

Thus the technique of measuring D_2 is essentially the following: The measurements are made by recording one variable of the system with successive values equally spaced in time. Then one plots the trajectory in a space whose coordinates are sequential values of the measured variable which are delayed from each other by equal amounts (not necessarily the time delay between successive points in the original data set). This procedure is called "embedding the time series" in a higher-dimensional space. In this embedding space one measures the relative separation of points to find out the correlation integral. The embedding theorem establishes conditions under which a sufficiently high-dimensional reconstruction properly recovers the topology of the attractor. Hence, if the extracted dimension converges for a range of embedding dimensions one can infer that it is the correlation dimension of the attractor. In calculations, one cannot take the limits. Instead, one takes the smallest ϵ not obscured by noise and the largest m one can compute in a reasonable amount of time.

It is assumed in the Grassberger-Procaccia method of analysis that the algorithm parameters have been chosen wisely to provide an appropriate reconstruction of the attractor in the new embedding space. If the "sampling time" τ_s (time interval between successive data points) is too small, information contained in successive components of the embedding vectors would be redundant. If τ_s is too large the components of the vectors would be too uncorrelated. If τ represents the appropriate time between the components of the vectors and $\tau_s > \tau$, then clearly smaller τ_s should be used. If $\tau_s < \tau$, then one should use values of the time series which are separated by appropriate time intervals by "skipping" over values of the time series in forming the successive components of each embedding vector. Determining an appropriate time scale is thus an important factor in this method of analysis. This method also presupposes that proper values of the embedding dimension are to be used to reconstruct the system's trajectory. Theorems due to Takens[32] and Mané[33] state that, in order to have a proper embedding,[34] the embedding dimension m and the dimension d should satisfy the inequality $m \geq 2d + 1$. Since d is normally not known a priori, the most effective choice of m is determined by trial and error—that is, by scanning m from small to large values and noticing the m value where slopes no longer increase with increasing m. However, the presence of noise in the data and the need to use high embedding dimensions may lead to overlap between the two "noisy regions" (small $\ln \epsilon$ and large $\ln \epsilon$). In this case no "plateau" may be observed.

Other dimension algorithms have been proposed by, e.g., Badii and Politi.[34] Studies by various authors[34] indicate that this method is rather more accurate than that of Grassberger and Procaccia for large-dimensional attractors. However, the Grassberger-Procaccia (GP) method has been used by some to find dimensions within 10–20 % accuracy for values up to 8. Because the GP method has been shown to be sufficient to identify noise in large-dimensional systems and because the methods of Badii and Politi typically require more data values than were available to us, we settled on the GP method as modified (see below) as sufficient for our purposes.

The procedure has been improved by Albano et al.[35] who adapted the GP method to a technique for finding the smallest Euclidean space in which a trajectory is embedded as well as the orthonormal basis vectors spanning this space. The basis vectors e_i are the eigenvalues of the "covariance matrix"

$$\mu_{ij} = \frac{1}{N} \sum_k X_i(k) X_j(k) ,$$

where

$$\mu e_i = \sigma_i^2 e_i .$$

The symmetries of μ are such that σ_i^2 are greater than or equal to zero and $e_i \cdot e_j = \delta_{ij}\sigma_i^2$ is the mean-square projection of the embedding vectors on the axis i in this basis. Here N is the total number of embedding vectors and $X_i(k)$ is the ith component of the kth embedding vector

$$\mathbf{X}(k) = (X_1(k), X_2(k), \ldots, X_m(k))$$

$$= (v(1+(k-1)J), v(1+(k-1)J+p), \ldots, v(1+(k-1)J+(m-1)p)) ,$$

where $v(t)$ represents the time series measured at sampling time intervals τ_s, p is the "lag" (number of sampling intervals between successive components of each embedding vector), and J is the number of sampling intervals between the first components of successive vectors. The time $(m-1)p$, spanned by each embedding vector, is called the "window length" of the embedding. Broomhead and King[36] suggested that an optimum window length is given by $1/\omega^*$, where ω^*, the band limiting frequency, is the highest frequency that significantly contributes to the power spectrum of the time series. Since the autocorrelation function and its power spectrum are Fourier transforms (Wiener-Khintchine theorem) of each other, the autocorrelation time and $1/\omega^*$ are of the same order of magnitude.

Thus in the Albano et al. method of analysis, starting from the time series, one forms the covariance matrix μ and calculates its eigenvalues and eigenvectors. Eigenvalues and eigenvectors are obtained by diagonalizing the covariance matrix by using the singular value decomposition technique. Since the matrix of the eigenvectors of μ is an orthogonal transformation of the embedding space, Euclidean distances between embedding vectors are preserved. The correlation integral and, hence, the correlation dimension are then invariant in the transformation. In the absence of noise the number of nonzero eigenvalues (that is the rank of the covariance matrix) is the dimension of the smallest subspace of the embedding space that contains the reconstructed trajectory. Since noise prevents any eigenvalues from becoming zero, dimension is actually estimated by computing the GP correlation integral in this new transformed space corresponding to a chosen embedding dimension m.

III. EXPERIMENTS AND RESULTS

The ASE signal was provided by a single multianode laser amplifier tube made of Pyrex of length 300 cm and of inner diameter 4 mm. The rube was dc excited by a 1–10 kV, 15 mA regulated power supply with a 300–750 ballast resistance in series to damp out any plasma oscillations. The experimental setup and measurement apparatus were as described elsewhere.[17] In order to get an inhomogeneously broadened medium the discharge tube was filled with 182 mTorr of 90% single isotope Xe-136. This resulted in a homogeneous linewidth of about 7 MHz compared with an inhomogeneous Doppler linewidth estimated to be about 110 MHz. For a more relatively homogeneously broadened medium the discharge tube was filled with 182 mTorr of Xe and 2.4 Torr of 99.9 wt. % He which provided a total homogeneously broadened linewidth of about 54 MHz. The discharge current used in the experiments was 3.7 mA — a low value was used in order to avoid cataphoresis. One
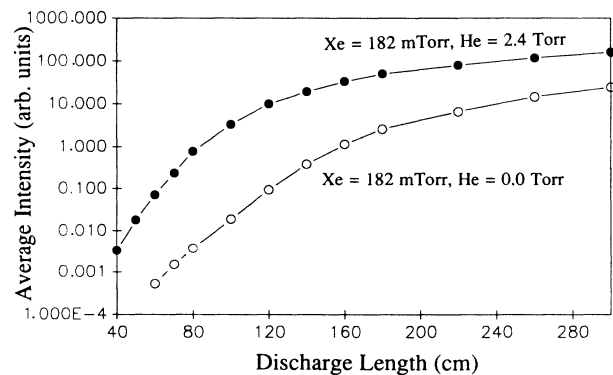

FIG. 1. Variation of average intensity with discharge length for the inhomogeneously broadened and the relatively homogeneously broadened ASE.

linearly polarized component of the 3.51-μm ASE signal was detected, amplified, and digitized using a fast transient recorder. A Tektronix fast digitizer was used in initial experiments providing ten-bit resolution and a maximum digitizing rate of 1 GHz but digitized sequences were limited to only 512 data points. For longer time series a Lecroy fast transient recorder (model TR8828C) was used providing eight-bit resolution, maximum digitizing rate of 200 MHz/sec (5-ns sampling time), and data sets of up to 128 000 points. We found special value in comparing the analysis of data from these two digitizers because they provide typical experimental compensating trade-offs among digitizing resolution, digitizing rate, and the length of the data stream. The average intensity of the ASE signal was recorded by chopping the ASE signal and using a lock-in amplifier. As a reference noise signal, the output from a Hewlard-Packard 461A amplifier was also digitized and used in the dimension analysis for comparison with the ASE results.

Variation of the average intensity with source length is shown in Fig. 1 for the inhomogeneously broadened and for the relatively homogeneously broadened cases, respectively. The less than exponential growth at longer discharge lengths indicates that the ASE signal is heavily saturated. This is also confirmed by the spectral rebroadening in the inhomogeneously broadened case and the significant decrease of the rebroadening rate[1] (not shown here) for the more homogeneously broadened case.

A FORTRAN program implementing the GP algorithm was used to compute the correlation integral of the embedding trajectories. In order to check the results, longer data sets were analyzed with different embedding dimensions and for data sets from different experimental conditions. As a cross check, we calculated the dimension using the method of Albano et al.[35] of projecting the embedded attractor onto subspaces spanned by its principal axes. The power spectrum (homodyne) of the ASE signal was obtained by fast Fourier transforming (and then squaring) the digitized intensity time series.

Figures 2(a) and 2(b) show the intensity time series and power spectrum, respectively, of a digitized homogeneously broadened (Xe = 182 mTorr, He = 1 Torr, current = 4 mA) ASE signal of 512 points taken at a sampling time of 10 ns with ten-bit resolution. Figures 2(c) and 2(d) show corresponding plots of slopes versus $\ln C_n$ for the GP correlation integral for embedding dimensions between 10, 12, 14, 16, 18, and 20 for different "lag" (time delays between components of a vector) values. The slopes increase steadily with increasing embedding dimension. However, though this data set had better resolution than the data sets analyzed in Figs. 3 and 4, it was limited to 512 data points which prohibited reconstruction of attractors with large embedding dimension and which inhibited variation of the parameters of the embedding. These limitations prevented us from drawing strong conclusions about the existence of an attractor from these analyses.

In Figs. 3 and 4 we show analyses of longer time series (5000 points) of lower (eight-bit) resolution taken with a Lecroy digitizer with a sample interval of 5 ns. The correlation time of these signals is about 20 ns.[17] A sam-
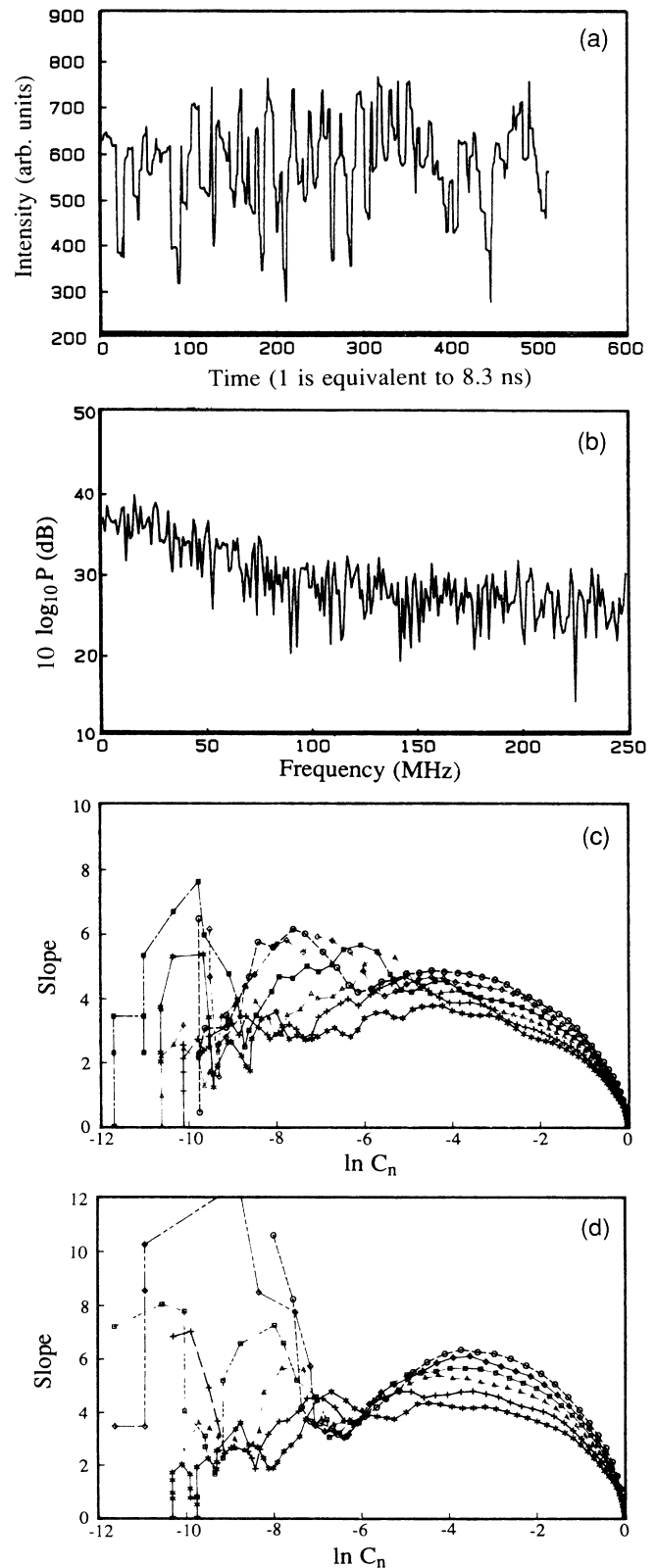

FIG. 2. (a) Intensity time series, (b) power p spectra of the ASE at discharge length of 180 cm for the relatively homogeneously broadened case (Xe = 182 mTorr, He = 1 Torr, current = 4 mA). (c) and (d): slope vs $\ln\epsilon$ for embedding lag = 1 and lag = 2, respectively, for embedding dimensions 10 to 20, in steps of 2. The base-line spectral density in (b) is caused by noise and the limited digitizing precision.
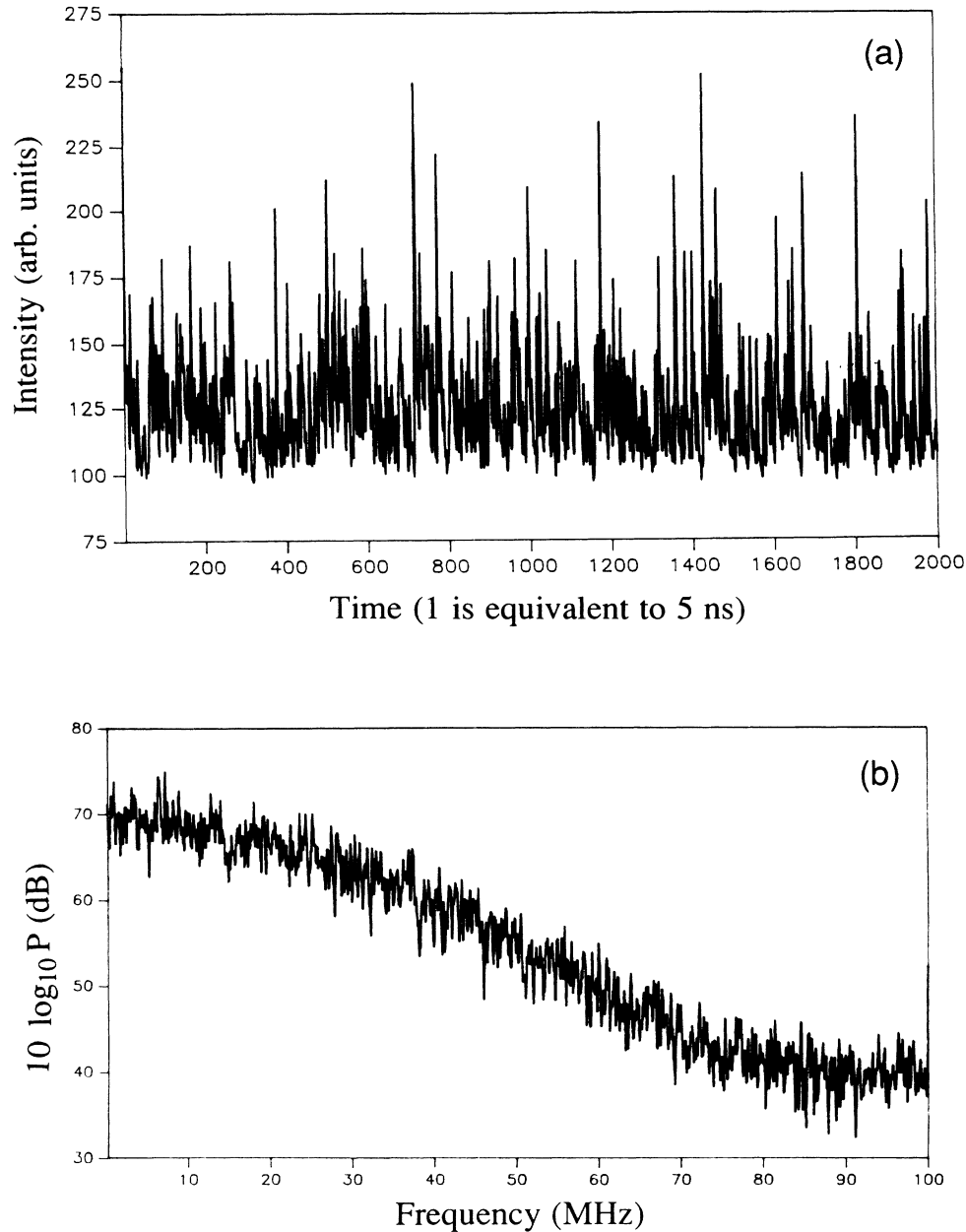
FIG. 3. (a) Intensity time series, (b) power spectra, (c) $\ln C_n$ vs $\ln\epsilon$, (d) slope vs $\ln C_n$, (e) slope vs $\ln\epsilon$ [(c)–(e) for embedding dimensions 2 to 20, in steps of 2], and (f) slope vs embedding dimension (for $\ln\epsilon = -3.0$) for the ASE signal from the inhomogeneously broadened case at a discharge length of 300 cm.

pling time interval of 5 ns clearly satisfies the criterion for proper embeddings. Figure 3(a) shows the intensity time series of the inhomogeneously broadened ASE signal obtained at 300-cm discharge length (29.1 unsaturated gain lengths). The power spectrum shown in Fig. 3(b) is clearly broadband. Figures 3(c)–3(e) show the plots of $\ln C_n$ versus $\ln\epsilon$, slope versus $\ln C_n$, and slope versus $\ln\epsilon$. In the analysis all embedding vectors are used for each embedding dimension in the computation of the GP correlation

integral. The length scale ϵ is normalized to the largest interpoint distance in each embedding. Again in this case the slope increases steadily with increasing embedding dimension. To see the nature of this variation, the values of the slopes obtained at a particular value of $\ln\epsilon$ are plotted versus the embedding dimension in Fig. 3(f).

Figure 4(a) shows the corresponding analysis of 4000 points of an intensity time series for the relatively homogeneously broadened ASE obtained at discharge length of
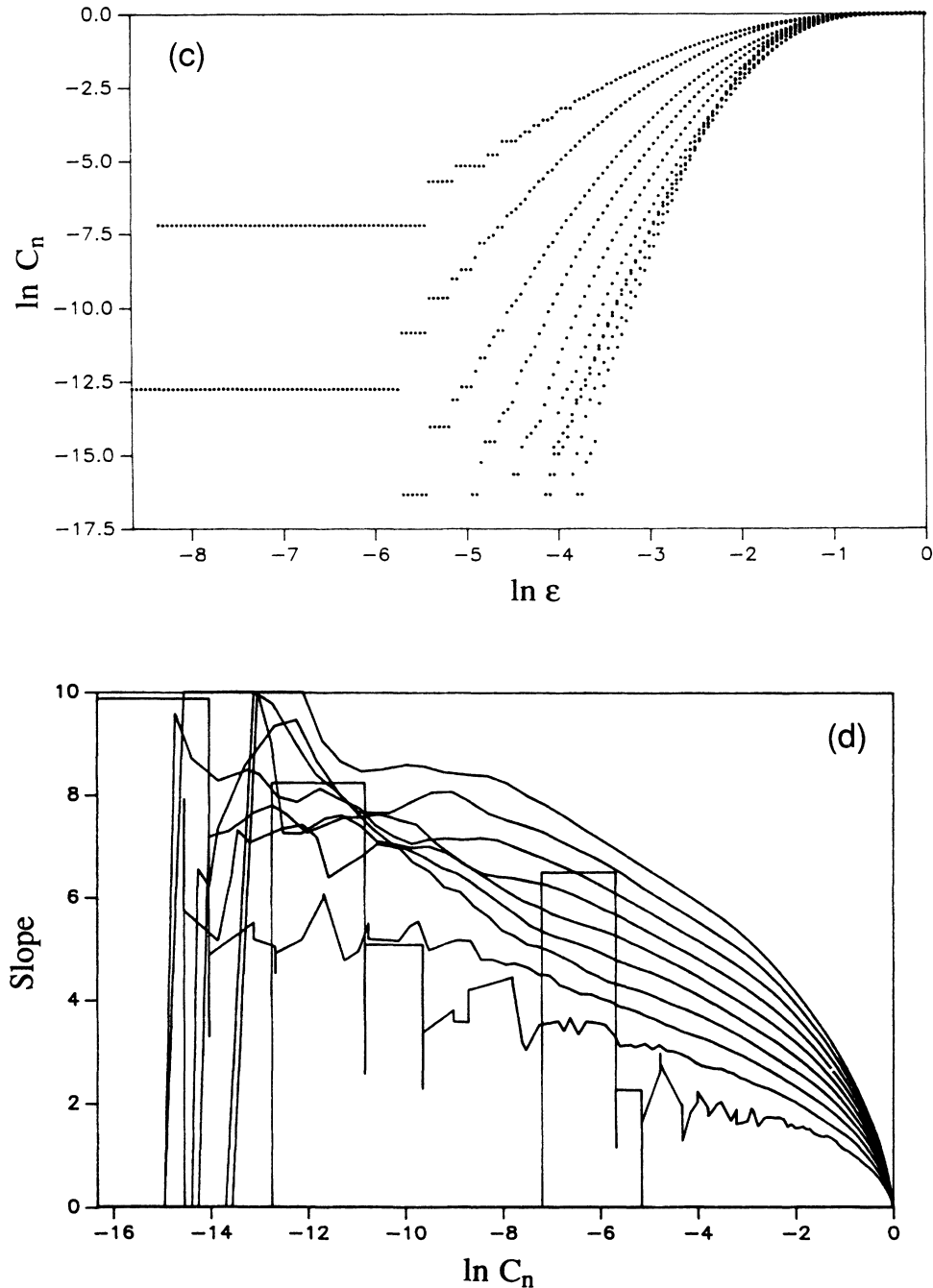
FIG. 3. (*Continued*).

300 cm (51 unsaturated gain lengths). Its broadband spectrum is shown in Fig. 4(b). Figures 4(c)–4(e) show the plots of $\ln C_n$ versus $\ln\epsilon$, slope versus $\ln C_n$, and slope versus $\ln\epsilon$. Here again the slope increases with increasing embedding dimension at a rate shown by the plot in Fig. 4(f).

The analyses were repeated with different data sets obtained under different experimental conditions with different sampling intervals ranging from 5–20 ns and for different lag values. In all such analyses the slopes always increased with increasing embedding dimension.

For comparison with the ASE results, digitized noise from the HP-461 video amplifier (cutoff frequency ~200 MHz) was also analyzed using the GP algorithm. The data set consisted of 5000 points of eight-bit resolution taken with a 5-ns sampling interval. Figure 5(a) shows the slope versus $\ln C_n$ for embedding dimensions 2 to 16 in steps of 2. In computations of the correlation integral all embedding vectors are used. The slope at any particular value of ϵ increases with the embedding dimension, as expected for random noise. The increase is seen as the positive slope in Fig. 5(b). Interestingly, the increase with
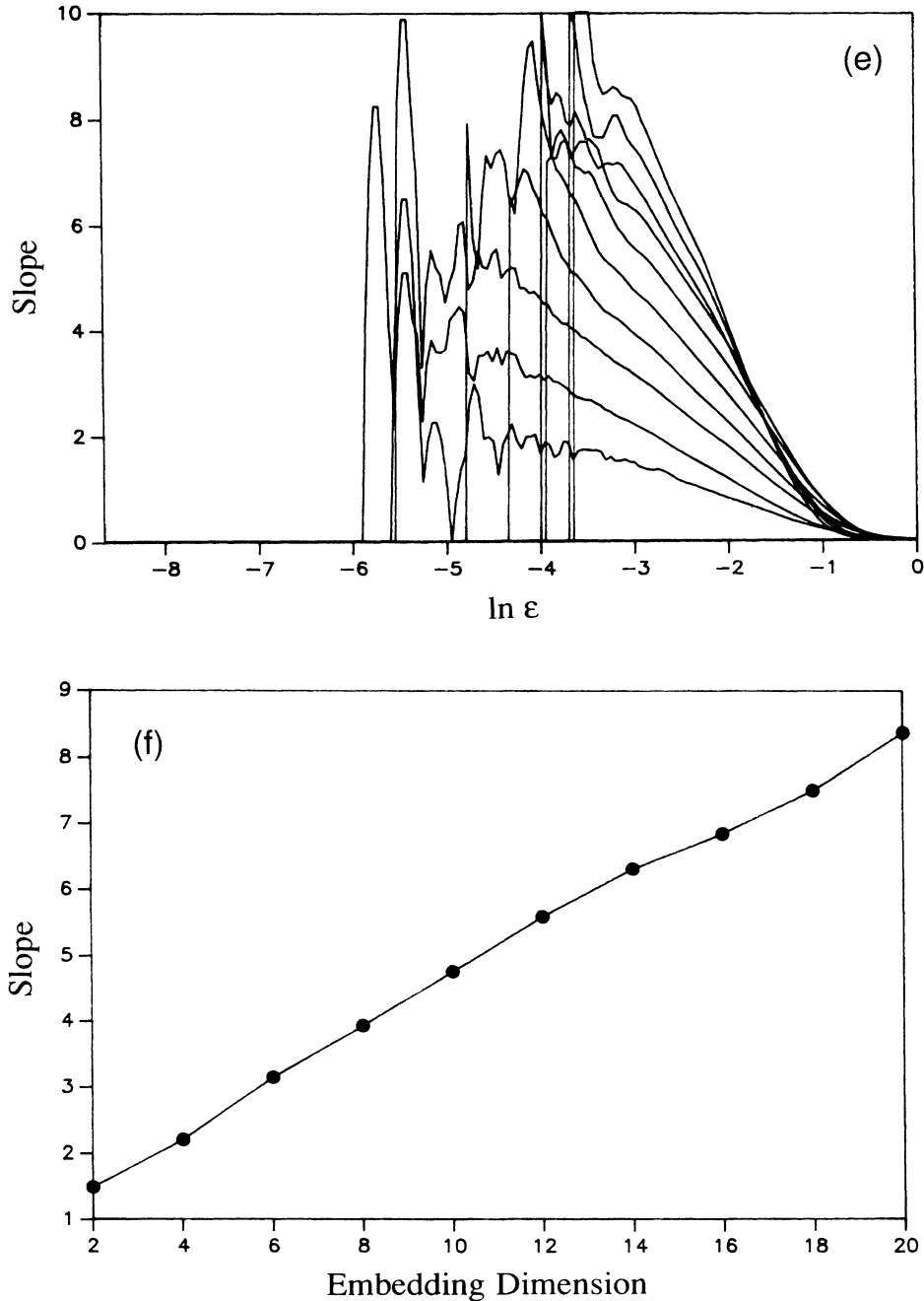
FIG. 3. (Continued).

embedding dimension in Fig. 5(b) for the amplifier noise is different from the increases for the ASE data sets shown in Figs. 3(f) and 4(f). The rates of increase for the two ASE data sets also differ among themselves. The rate of increase with embedding dimension correlates with the spectral bandwidth, being lowest for the relatively homogeneously broadened ASE (40 MHz) while it is greatest for the amplifier noise (200 MHz). This clarifies one of the subtleties of the dimension calculations. One should expect an increase of the apparent attractor dimension with increasing embedding dimension for colored noise to be related to the ratio of the time delay between com-

ponents of a vector (the lag) to the correlation time of the signal.

Even longer data sets were analyzed using the improved method of Albano et al.[35] Figure 6 provides the results of analysis of a data set of 100 000 points sampled at 5-ns intervals with eight-bit resolution for the relatively homogeneously broadened ASE obtained at discharge length 300 cm. The 100 000 points were used to construct 10 000 vectors. Choosing 10 to be the embedding dimension, a singular value decomposition was performed to find the principal axes of embedding. Embedding vectors were selected uniformly from the entire data
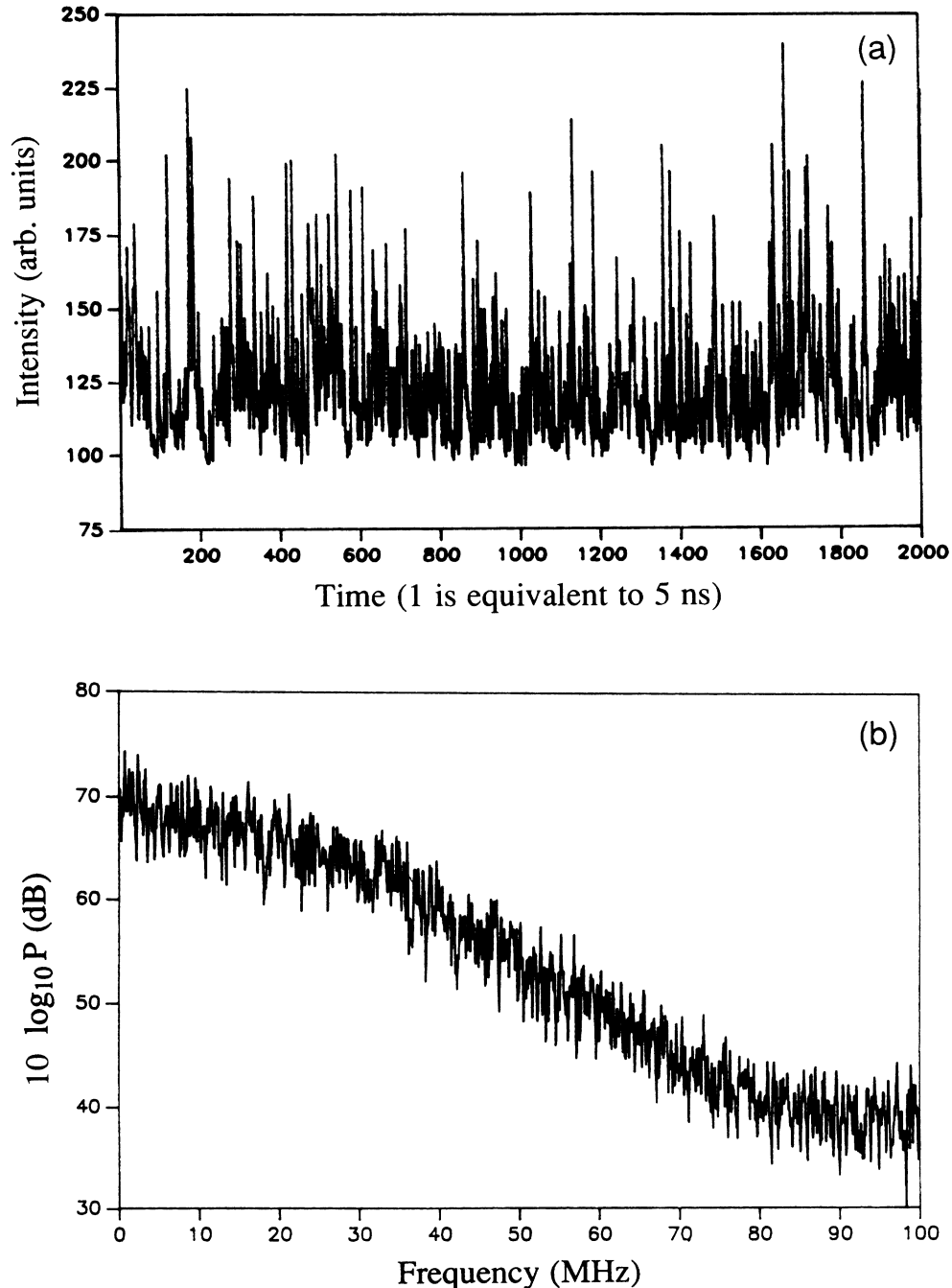
FIG. 4. (a) Intensity time series, (b) power spectra, (c) $\ln C_n$ vs $\ln \epsilon$, (d) slope vs $\ln C_n$, (e) slope vs $\ln \epsilon$ [(c)–(e) for embedding dimensions 2 to 20, in steps of 2], and (f) slope vs embedding dimension (for $\ln \epsilon = -3.0$) for the ASE from the relatively homogeneously broadened case at a discharge length of 300 cm.

set. The normalized eigenvalues of the singular value analysis were 0.396, 0.267, 0.173, 9.15×10^{-2}, 4.25×10^{-2}, 1.70×10^{-2}, 7.57×10^{-3}, 3.14×10^{-3}, 1.50×10^{-3}, and 8.94×10^{-4}. The trajectory matrix was then rotated to get the matrix of the principal components which was then used to calculate the GP correlation integral. Figure 6(a) shows the slope of the correlation integral versus $\ln \epsilon$ for subspaces 7, 8, 9, and 10. Fig-

ure 6(b) shows the same plot for a subset of the same data set where 10 000 points were used to construct 1000 vectors. The embedding dimension was chosen to be 5 and the calculation was done for subspaces 3, 4, and 5. Figure 6(c) shows the same plot for a different data set of the relatively homogeneously broadened ASE at the same discharge length 300 cm. This data set also has eight-bit resolution and sampled at 5-ns intervals. In the analysis
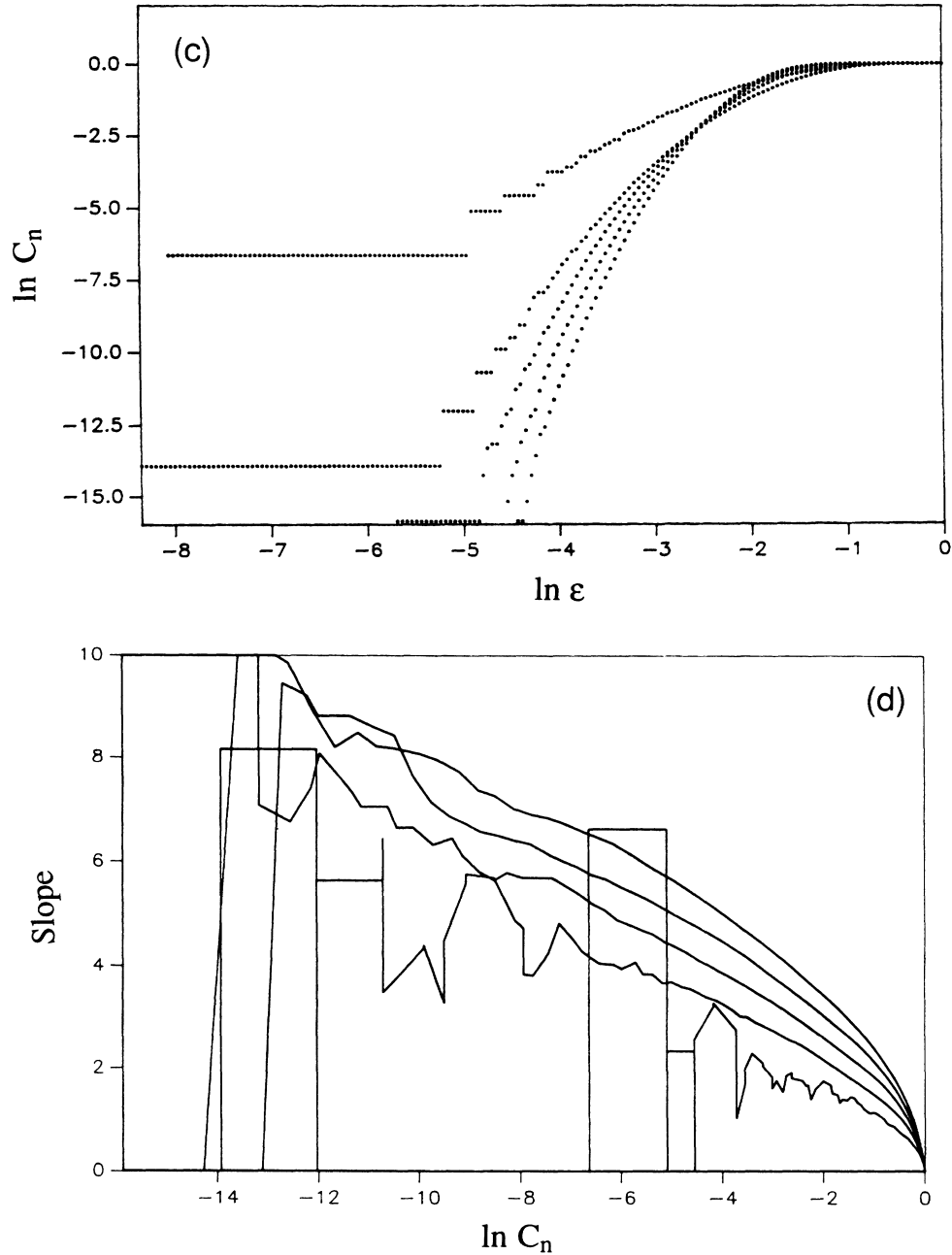
FIG. 4. (Continued).

100 000 points are used to construct 9000 vectors. The embedding dimension was chosen to be 11 and the calculation was done for subspaces 8, 9, 10, and 11. Normalized eigenvalues are 0.373, 0.282, 0.169, 9.25×10^{-2}, 4.57×10^{-2}, 2.08×10^{-2}, 8.84×10^{-3}, 3.95×10^{-3}, 2.19×10^{-3}, 1.33×10^{-3}, and 9.95×10^{-4}.

Figure 7(a) shows a plot of slope versus $\ln\epsilon$ for a data set from the inhomogeneously broadened ASE where in the analysis 100 000 points were used to construct 10 000 vectors. The data set was taken at the discharge length 300 cm (gain length 29.1) with the same sampling time interval of 5 ns. The embedding dimension was 10 and results for subspaces 7, 8, 9, and 10 are shown. The nor-

malized eigenvalues were 0.413, 0.260, 0.171, 8.73×10^{-2}, 4.14×10^{-2}, 1.64×10^{-2}, 6.52×10^{-3}, 2.52×10^{-3}, 1.11×10^{-3}, and 6.83×10^{-4}. Figure 7(b) shows a similar plot of slope versus $\ln\epsilon$ for a different data set of the inhomogeneously broadened ASE obtained at the discharge length 180 cm (gain length 17.5). This data set also had eight-bit resolution and sampling time 5 ns. 100 000 points were used to construct 9000 vectors. The embedding dimension was 11 and the calculation was done for the subspaces 8, 9, 10, and 11. Normalized eigenvalues are 0.487, 0.239, 0.139, 6.95×10^{-2}, 3.24×10^{-2}, 1.34×10^{-2}, 6.64×10^{-3}, 4.22×10^{-3}, 3.57×10^{-3}, 2.87×10^{-3}, and 2.55×10^{-4}.
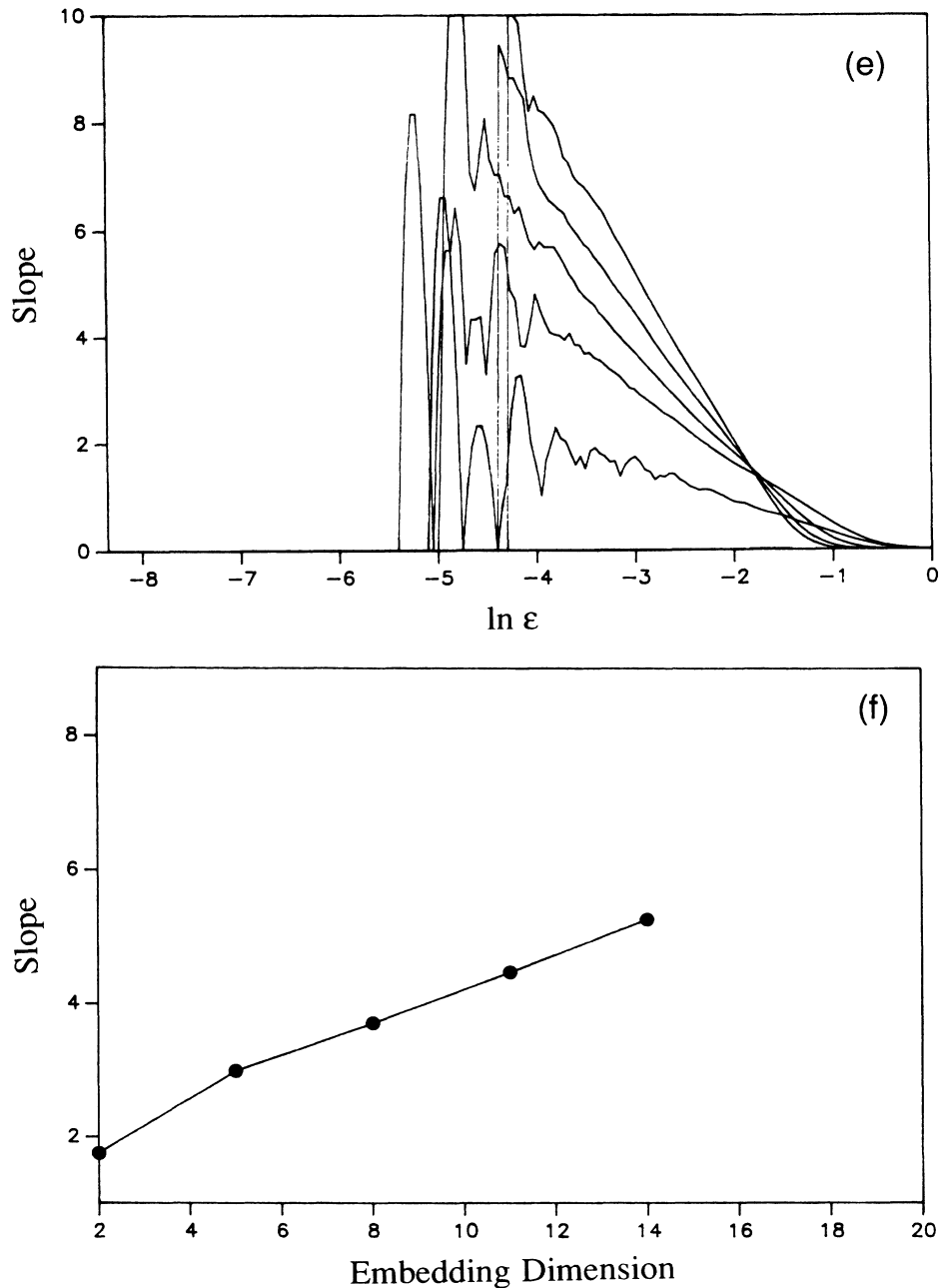
FIG. 4. (Continued).

In all three cases there is no "plateau" in the slope which would be indicative of a dimension and thereby indicating the existence of an attractor. Instead, the slope increases with embedding dimension which is characteristic of noise. The convergence of the slope curves for larger values of ϵ may indicate that there is some characteristic density distribution of the embedded data sets on larger length scales, but it is not that of a fractal set.

IV. DISCUSSION

We conclude that there is no evidence of a low-dimensional strange attractor as a cause for the ASE in-

tensity fluctuations with broadband power spectra and irregular time series from the heavily saturated 3.51-μm source. The slopes of the correlation integrals do not converge to show any common plateau for any of the conditions. Instead, the slopes always increase with increasing embedding dimension—a behavior observed and expected for stochastic random noise. Thus there is no evidence of a fractal dimension which would be expected for a deterministic chaotic system.

One might have expected some deterministic features in the case of ASE caused by the coherent evolution and ringing after the intense pulses. Instead, the absence of any common plateau in the plots of the correlation in-
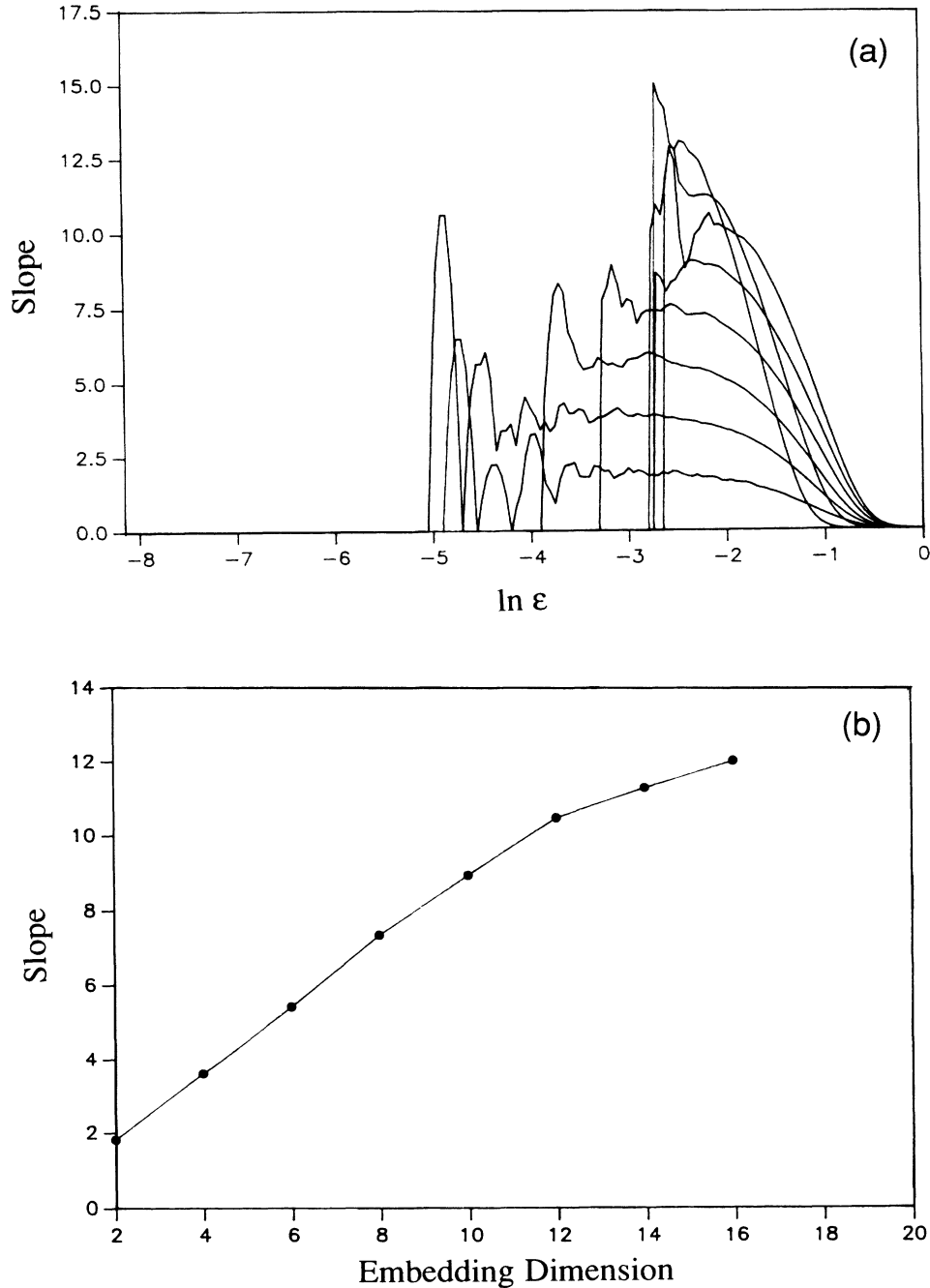
FIG. 5. (a) Slope vs $\ln C_n$ for embedding dimensions 2 to 16, step 2 and (b) slope vs embedding dimension (for $\ln \epsilon = -2.2$) for electronic noise from a HP-461A amplifier (flat from 1 kHz to 150 MHz).

tegrals, obtained from a wide range of operating conditions, makes it clear that the broadband fluctuations in the heavily saturated ASE are associated with a stochastic state for which the concept of correlation dimension does not have any meaning or, even if it does, it is not discernible with the present techniques of analysis even when the analysis is carried out in reconstructed subspaces of dimension up to 20 (the maximum embedding dimension used in the computations).

It is noteworthy, in this connection, that this type of

noisy origin of the broadband fluctuations of heavily saturated ASE sharply contrasts with that of the low-dimensional chaotic output of unstable 3.51-μm xenon lasers.[25,37,38] In the lasers there is a clear evidence of fractal dimensions between 2 and 3 for data sets with broadband optical power spectra similar to those of the ASE signals. However, though they both have broadband spectra they differ in other ways. One difference is in their autocorrelation functions. The intensity autocorrelation functions for the chaotic laser signals show
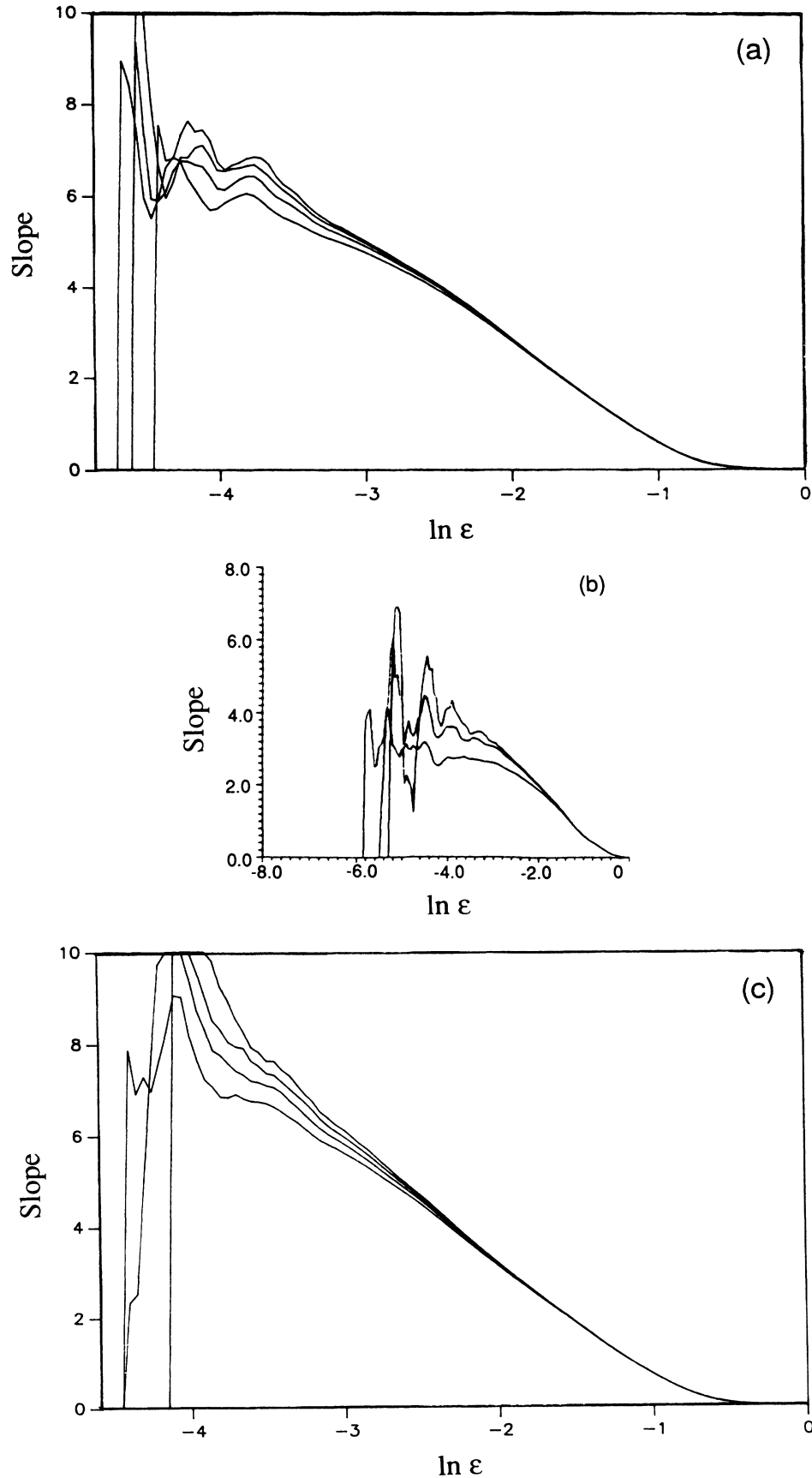
FIG. 6. Slope vs lnϵ for (a) embedding space 10, subspaces 7–10, (b) embedding space 5, subspaces 3–5, and (c) for embedding space 11, subspaces 8–11 for the relatively homogeneously broadened ASE at discharge length 300 cm.
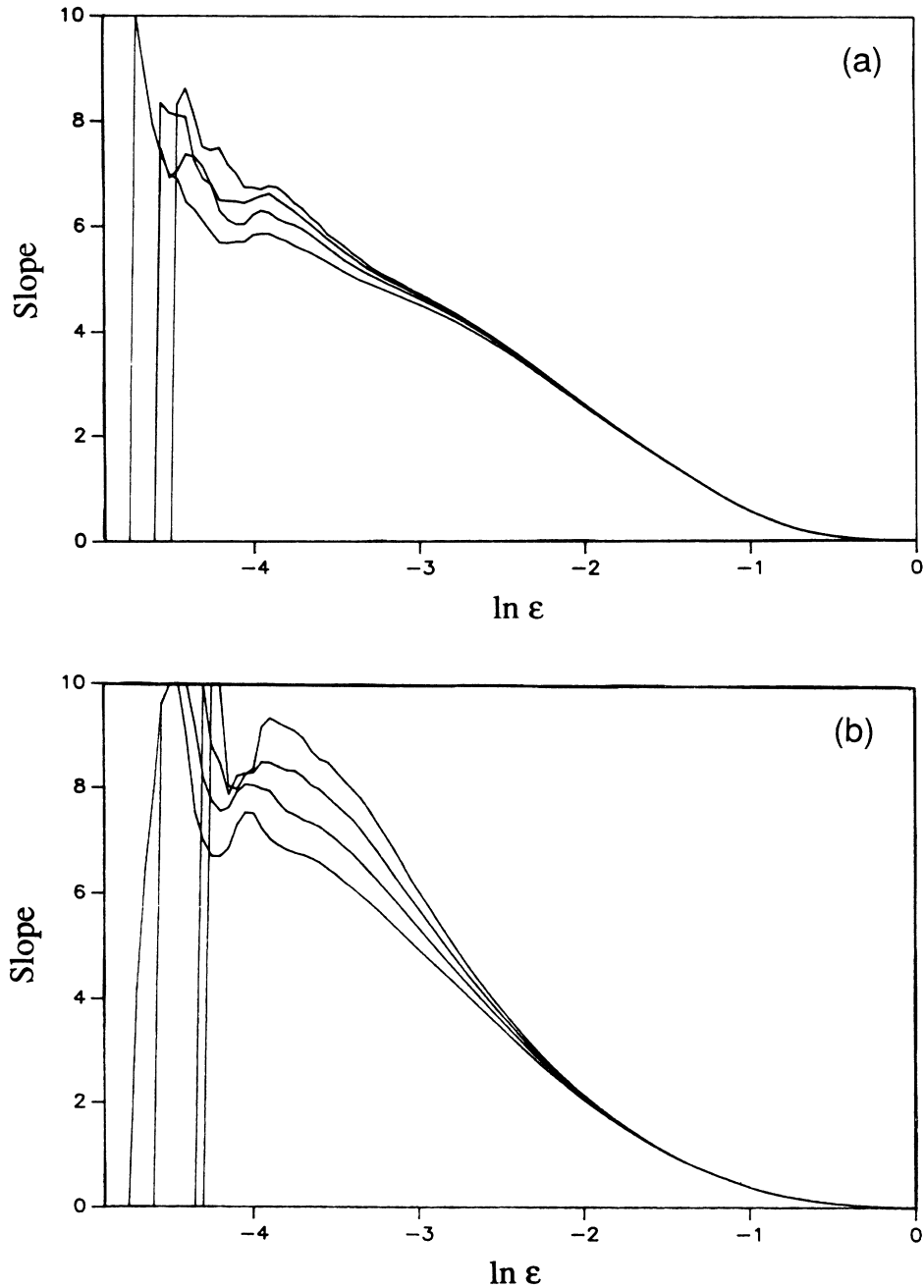
FIG. 7. Slope vs $\ln\epsilon$ for (a) embedding space 10, subspaces 7–10 at discharge length 300 cm and (b) embedding space 11, subspaces 8–11 at discharge length 180 cm for the inhomogeneously broadened ASE.

clear ringing and a slow decay of the envelope instead of single-peaked, rapidly decaying results for the ASE.[1,17] The chaotic lasers also differ from the ASE in their intensity probability distribution functions. However, there are forms of fully developed chaos which would not be distinguishable from the ASE based on spectra, correlation functions, or probability distributions. Thus the computation of quantities such as correlation dimension and autocorrelation functions enables us to unambiguously discriminate low-dimensional chaos from these randomly fluctuating intensities. We conclude that in this case stochastic processes underlie the long-term evolution of ASE signals.

*Present address: Department of Physics, University of Nevada, Las Vegas, 4505 Maryland Parkway, Las Vegas, NV 89154.

[1] B. Das, Ph.D. thesis, Bryn Mawr College, 1988, available from University Microfilms.

[2] L. W. Casperson and A. Yariv, IEEE J. Quantum Electron. **QE-8**, 80 (1972).

[3] L. W. Casperson, J. Appl. Phys. **48**, 256 (1977).

[4] H. Maeda and A. Yariv, Phys. Lett. **43A**, 383 (1983).

[5] D. H. Schwamb and S. R. Smith, Phys. Rev. A **23**, 896 (1980).

[6] R. W. Gray and L. W. Casperson, IEEE J. Quantum Electron. **QE-14**, 893 (1978).

[7] H. Gamo and H. Osada, *Coherence and Quantum Optics IV*, edited by L. Mandel and E. Wolf (Plenum, New York, 1975), p. 583.

[8] F. A. Hopf, IEEE J. Quantum Electron. **QE-10**, 717 (1974).

[9] D. C. Newitt and N. B. Abraham, Opt. Commun. **31**, 393 (1979).

[10] N. B. Abraham and E. B. Rockower, Opt. Acta **26**, 1297 (1979).

[11] N. B. Abraham, D. Kranz, J. Huang, and E. B. Rockower, Phys. Rev. A **24**, 2556 (1981).

[12] B. Das and N. B. Abraham (unpublished).

[13] B. Das, G. Alman, N. B. Abraham, and E. B. Rockower, Phys. Rev. A **39**, 5153 (1989).

[14] N. B. Abraham, Phys. Rev. A **21**, 1595 (1980).

[15] N. B. Abraham and S. R. Smith, Opt. Commun. **38**, 372 (1981).

[16] S. P. Adams and N. B. Abraham, in *Coherence and Quantum Optics V*, edited by L. Mandel and E. Wolf (Plenum, New York, 1984), p. 233.

[17] B. Das and N. B. Abraham (unpublished).

[18] N. B. Abraham, A. M. Albano, B. Das, T. Mello, M. F. H. Tarroja, N. Tufillaro, and R. S. Gioggia, in *Optical Chaos*, Proceedings of the International Society for Optical Engineering, Bellingham, WA, 1986, edited by J. Chrostowski and N. B. Abraham [Proc. Soc. Photo-Opt. Instrum. Eng. **667**, 2 (1986)].

[19] F. A. Hopf, Phys. Rev. Lett. **56**, 2800 (1986); private communication.

[20] E. N. Lorenz, J. Atmos. Sci. **20**, 130 (1963).

[21] B. A. Huberman and J. P. Crutchfield, Phys. Rev. Lett. **43**, 1743 (1979).

[22] J. P. Gollub and H. Swinney, Phys. Rev. Lett. **35**, 927 (1975).

[23] J. P. Gollub and S. V. Benson, J. Fluid Mech. **100**, 449 (1980).

[24] N. B. Abraham, J. P. Gollub, and H. S. Swinney, Physica D **11**, 252 (1984).

[25] A. M. Albano, J. Abounadi, T. H. Chyba, C. E. Searle, S. Yong, R. S. Gioggia, and N. B. Abraham, J. Opt. Soc. Am. B **2**, 47 (1985).

[26] M. W. Derstine, H. M. Gibbs, F. A. Hopf, and D. L. Kaplan, Phys. Rev. A **27**, 3200 (1983).

[27] N. B. Abraham, A. M. Albano, B. Das, T. Mello, M. F. H. Tarroja, and N. Tufillaro, in Ref. 18, p. 2.

[28] J. D. Farmer, Physica D **4**, 566 (1982).

[29] P. Grassberger and I. Procaccia, Phys. Rev. A **28**, 2591 (1983); Phys. Rev. Lett. **50**, 346 (1983); A. Ben Mizrachi, I. Procaccia, and P. Grassberger, Phys. Rev. A **29**, 975 (1984).

[30] J. D. Farmer, E. Ott, and J. A. Yorke, Physica D **7**, 153 (1983).

[31] P. Grassberger and I. Procaccia, Physica D **13**, 34 (1984).

[32] F. Takens, in *Dynamical Systems and Turbulence*, edited by D. A. Rand and L. S. Young (Springer, Berlin, 1981), p. 365.

[33] R. Mané, in *Lecture Notes in Mathematics*, edited by D. A. Rand and L. S. Young (Springer-Verlag, Berlin, 1981); see also J.-P. Eckmann and D. Ruelle, Rev. Mod. Phys. **57**, 617 (1985).

[34] R. Badii and A. Politi, J. Stat. Phys. **40**, 725 (1985).

[35] A. M. Albano, J. Muench, C. Schwartz, A. I. Mees, and P. E. Rapp, Phys. Rev. A **38**, 3017 (1988).

[36] D. S. Broomhead and G. P. King, Physica D **10**, 217 (1986).

[37] N. B. Abraham, A. M. Albano, D. K. Bandy, B. Das, G. de-Guzman, T. Issacs, M. F. H. Tarroja, S. Yong, S. P. Adams, and R. S. Gioggia, in *Optical Instabilities*, edited by R. W. Boyd, M. G. Raymer, and L. M. Narducci (Cambridge University Press, Cambridge, 1985), p. 224.

[38] N. B. Abraham, A. M. Albano, B. Das, and M. F. H. Tarroja, in *Fundamentals of Quantum Optics II*, edited by F. Ehlotzky (Springer-Verlag, Berlin, 1987), p. 32.